Electron Paramagnetic Resonance Spectroscopy of Iron(III)-Doped MFI Zeolite. 1. Multifrequency CW-EPR

A. M. Ferretti,[†,‡] A.-L. Barra,[§] L. Forni,[†] C. Oliva,[†] A. Schweiger,[∥] and A. Ponti*,[⊥]

Università di Milano, Dipartimento di Chimica Fisica ed Elettrochimica, via C. Golgi 19, I-20133 Milano, Italy, Centre National de la Recherche Scientifique, Laboratoire des Champs Magnétiques Intenses, F-38042 Grenoble, France, Laboratorium für Physikalische Chemie, ETH Hönggerberg, HCI, CH-8093 Zürich, Switzerland, and Consiglio Nazionale delle Ricerche, Istituto di Scienze e Tecnologie Molecolari, via C. Golgi 19, I-20133 Milano, Italy

Received: October 9, 2003; In Final Form: December 11, 2003

Iron-containing zeolites with MFI structure are effective catalysts for several important reactions, among which the one-step hydroxylation of benzene to phenol by N_2O stands out. We report on a multifrequency (9−475 GHz) continuous-wave electron paramagnetic resonance (CW-EPR) study of an Fe(III)-doped MFI zeolite catalyst either as synthesized and after detemplation, steaming, and treatment by aqueous dithionite. The presence of substantial inhomogeneity of the zero-field splitting (ZFS) interaction has been recognized and a novel computational strategy has been implemented to fit the spectroscopic results. This procedure enabled us to obtain quantitative measures of the ZFS distribution features and to draw structural conclusions regarding the nature and environment of Fe(III) ions in the as-synthesized catalyst and after each treatment.

Introduction

Iron-containing zeolites with MFI structure have attracted considerable interest since 1988, when three groups of researchers[1−3] independently found that these materials are effective catalysts in the one-step hydroxylation of benzene to phenol by N_2O, a process much less expensive and less troublesome than the three-step cumene process.[4] Since Fe(III) is a fundamental constituent of the catalyst,[4−6] electron paramagnetic resonance (EPR) spectroscopy has been widely applied to these systems to study the nature and the environment of the iron ions.[5,7−26]

The EPR spectrum of Fe(III) ions in zeolites and related materials is sufficiently determined by a spin Hamiltonian including the electron Zeeman and the zero-field splitting (ZFS) interactions for a high-spin d^5 ion. The ZFS is sensitive to the environment of the Fe(III) ion because of its dependence on the ligand field that interacts with the d electrons.[27] The X-band EPR spectrum of iron-doped zeolites and silicalites usually comprises several lines. A group of lines is observed at low resonance field, i.e., at $g_{eff} \geq 4$ with a prominent peak at $g_{eff} = 4.3$ and several other ones down to $g_{eff} \cong 9$. Two major broad lines are found at $g_{eff} \cong 2.0$ and 2.3, the two peaks being largely superimposed. Other minor features are observed, including a peak very close to zero field ($g_{eff} \geq 10$). The conventional attribution is as follows:[7,8,11,13,17−19,21,23−25] the $g_{eff} \geq 4$ group is due to isolated Fe(III) ions in the zeolitic framework which suffer from various degrees of distortion and the $g_{eff} \cong 2.0$ and 2.3 lines arise from oxidic iron clusters and particles where Fe(III) ions strongly interact with each other (earlier interpretations[7,8,10] attributed the $g_{eff} \cong 2.0$ to extraframework ions in octahedral symmetry). However, this interpretation often disagrees with data from other techniques.[12] Indeed, there is convincing evidence[9,10,12,22] that both framework and extraframework Fe(III), either as isolated ions or as aggregates (oligo-nuclear clusters, oxidic particles), can contribute to each of the above spectral features. In other words, there is not a one-to-one correspondence between spectral features and iron species.

This difficulty can be traced back to the existence of a *distribution* of the ZFS interaction parameters and the consequent extensive spectral overlap. This distribution is expected in inhomogeneous systems such as iron-doped zeolites, especially after high-temperature treatments.[26] Indeed, many different intra- and extra-lattice sites are possible for Fe(III) ions. The latter include sites within the channels and on the external surface of the crystallites either as isolated ions or oxidic aggregates. Many framework sites are also possible: there are 12 or 24 different tetrahedral sites in the perfect lattice, depending on temperature and the presence of a template,[28,29] and additional inhomogeneity arises from the random distribution of aluminum ions and of lattice defects. Therefore, a new strategy to attack this problem is in order. First, there not being a clear correspondence between spectral features and iron species and environment, the entire spectrum must be simulated or, better, fitted to a spectral model. Second, such a model must include an explicit probability distribution function[30] of the ZFS interaction parameters that permits the evaluation of the degree of inhomogeneity of this interaction. Perhaps this is the only reliable piece of information that can be extracted from the continuous-wave (CW) EPR spectra of iron-doped zeolites.

In this paper we present a multifrequency CW-EPR study of iron-doped zeolite catalysts with MFI structure that undergo three sequential treatments, described in the following paragraph, necessary to improve conversion and selectivity of the catalyst[31] in the hydroxylation of benzene to phenol by N_2O. We report on EPR spectroscopy at 9.39 (X-band), 35.2 (Q-band), and

[†] Università di Milano.
[‡] Present address: Laboratorio MDM, Istituto Nazionale di Fisica della Materia, via C. Olivetti 2, I-20041, Agrate Brianza (MI), Italy.
[§] Centre National de la Recherche Scientifique.
[∥] ETH Hönggerberg.
[⊥] Consiglio Nazionale delle Ricerche.
* Corresponding author.

10.1021/jp0370371 CCC: $27.50
Published on Web 01/17/2004

several frequencies between 95 and 475 GHz. The key point of the present work is the definition and implementation of a spectral *fitting* (not merely simulating) procedure based on a model that entails a distribution of the ZFS interaction parameters. Application of this procedure to spectra rich in features (i.e. those observed at X-band) allows one to discuss the degree of inhomogeneity and disorder of the environment of the Fe(III) ions and to follow the variations induced by the various treatments the samples undergo. The difficulty of this approach is the severe computational burden one has to face, as the computation of the EPR spectrum of Fe(III) ions in zeolite requires two nested integrations. First, as zeolite samples are microcrystalline powders, the orientational "powder" integration must be performed, a process well-known in magnetic resonance spectroscopy.[32−34] Second, an average over the ZFS interaction, weighted by the chosen model distribution, has to be carried out. How the computational problem has been overcome is detailed below.

Experimental Section

The iron-doped MFI catalyst has been synthesized by the hydrothermal method.[35,36] The gel contains tetraethyl orthosilicate, triisopropoxylaluminum, and Fe(III) nitrate. After gel formation very pure tetrapropylammonium hydroxide has been added as templating agent. By this method, the iron ions substitute for silicon in the framework, as shown by X-ray powder diffraction patterns.[36] After careful washing with water, the "as-synthesized" catalyst (ZAS) is obtained. The catalyst has undergone several sequential treatments to get the catalytically active form. Detemplation is carried out by heating the catalyst by 0.5 K/min up to 393 K in nitrogen flow and then calcining in for 16 h at 823 K in air flow. To get the protonated form of the zeolite, detemplation has been followed by ion exchange, first with an aqueous solution of NH_4NO_3 and then with aqueous HNO_3. The catalyst has then been calcined at 823 K in air flow. At this step the catalyst is labeled ZDT. Next, the catalyst is subjected to a flow of 3:1 mol/mol steam/nitrogen mixture at 823 K for 6 h (ZST). This treatment extracts part of the iron ions from the lattice. It is thought that, during this treatment, and especially for high-Fe zeolites, iron ions may form large oxidic aggregates that hinder reactants diffusion in the zeolitic channels. To disperse these agglomerates, the catalyst has been washed with an aqueous solution of $Na_2S_2O_4$ and NaCl, followed by ion exchange and calcination as described above (ZCT).

The X-band spectra have been recorded with a Bruker ElexSys E500 spectrometer at 9.4 GHz, with 20 mW microwave power and 0.4 mT modulation amplitude in the temperature range from 110 to 390 K. The Q-band spectra have been recorded with an homemade spectrometer[37] at 35.2 GHz, with 10 mW microwave power and 0.4 mT modulation amplitude in the temperature range from 50 to 270 K. The high-frequency (95 to 475 GHz) spectra have been recorded in the temperature range from 5 to 100 K and with $2 \div 4$ mT modulation amplitude with a power below 1 mW at the sample for the lowest frequencies (95 and 115 GHz) and even smaller for the higher harmonics.

Description of the Fitting Procedure. The EPR spectrum of high-spin ($S = {}^5/_2$) Fe(III) ions in zeolites can be described by the Hamiltonian

$$\hat{H} = g\beta \mathbf{S}\cdot\mathbf{B}_0 + D[S_z^2 - {}^1/_3 S(S+1)] + E(S_x^2 - S_y^2) \quad (1)$$

where $g \cong g_e$ since high-spin Fe(III) is a ^6S ion, $\mathbf{B}_0$ is the static magnetic field vector, $D = 3D_z/2$, $E = (D_x - D_y)/2$, and D_i ($i = x, y, z$) are the principal values of the ZFS interaction, which are ordered so that $|D| \geq |E/3|$ and $D\cdot E \leq 0$.[38] For future convenience we also define the dimensionless parameter $\lambda = 3|E/D|$, $0 \leq \lambda \leq 1$.

As discussed above, the calculation of the EPR spectrum of Fe(III) ions in zeolite requires two different averages. For the orientational average, the spiral method[32] has been used. The distribution of interaction parameters in disordered systems has been discussed in detail[30] in the context of Mössbauer spectroscopy in relation to the distribution of electric field gradients, which determines the nuclear quadrupole splittings. Due to the formal and physical similarity of the ZFS and nuclear−quadrupole interactions, most results can be easily translated to the field of EPR spectroscopy of $S > {}^1/_2$ systems. The most studied case is that of the Gaussian isotropic model,[39] where all five components of the interaction tensor are normally distributed and statistically independent and the distribution of the principal axes of the interaction tensor is isotropic (statistical isotropy). Then the D and λ parameters are distributed as

$$C_5(D,\lambda) = \frac{3}{2\sqrt{2\pi}\sigma_5^5} D^4 \lambda \left(1 - \frac{\lambda^2}{9}\right) \exp\left(-\frac{D^2(1+\lambda^2/3)}{2\sigma_5^2}\right) \quad (2)$$

where σ_5 is a measure of the spread of the distribution. This distribution is completely defined by σ_5, however, it can be further characterized as follows. If $C_5(D,\lambda)$ is integrated over $0 \leq \lambda \leq 1$, the resulting marginal D distribution peaks at $D_{peak} \cong 1.8671\sigma_5$. If it is integrated over all possible D values, the resulting λ distribution has average $\langle\lambda\rangle \cong 0.6098$ and standard deviation $\sigma_\lambda \cong 0.2427$. The C_5 distribution has already been used in the simulation of the EPR spectrum of Fe(III) ions in borate glass.[40]

If it is assumed that not all interaction matrix elements are statistically independent, it follows that the interaction is also no more statistically isotropic. The distributions derived under this assumption are called degenerate Gaussian models[30] C_n, where $n < 5$ is the number of statistically independent elements. The importance of such models is that they are consistent with the existence of medium-range order about the probe ions.[41] In particular, the C_3 distribution,

$$C_3(D,\lambda) = \frac{9}{2(15-8\sqrt{3})} \frac{1}{\sqrt{2\pi}\sigma_3^3} D^2 \lambda \left(1 - \frac{\lambda^2}{9}\right) \exp\left(-\frac{D^2(1+\lambda^2/3)}{2\sigma_3^2}\right) \quad (3)$$

where σ_3 is a measure of the spread of the distribution, has already been applied to studies of local order by EPR spectroscopy of Fe(III) ions in fluoride[40,42−44] and phosphate[45] glasses. Note that σ_5 and σ_3 are not directly comparable. Integrating $C_3(D,\lambda)$ as above, we obtain that the marginal D distribution peaks at $D_{peak} \cong 1.3157\sigma_3$, and that the marginal λ distribution has average $\langle\lambda\rangle \cong 0.5902$.

Last, in some EPR studies[40,45] it was assumed that the D and λ parameters themselves are distributed according to a Gaussian law, either correlated or uncorrelated. When D and λ are uncorrelated, the Gaussian distribution is

$$G(D,\lambda) = \frac{1}{2\pi\sigma_D\sigma_\lambda} \exp\left[-\frac{(D-\bar{D})^2}{2\sigma_D^2}\right] \exp\left[-\frac{(\lambda-\bar{\lambda})^2}{2\sigma_\lambda^2}\right] \quad (4)$$

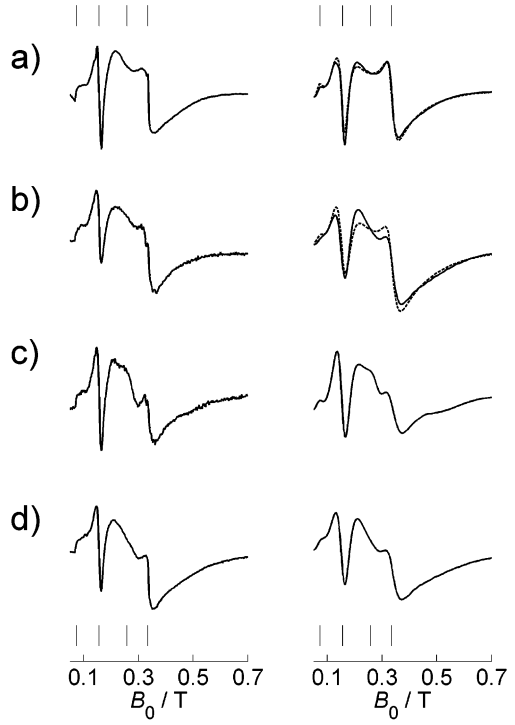

Figure 1. X-band EPR spectroscopy of Fe(III)-doped MFI zeolite at various stages of the treatment sequence: (a) ZAS; (b) ZDT; (c) ZST; and (d) ZCT. (Left) Experimental spectra recorded at 110 K (other conditions can be found in the text). (Right) Corresponding computed spectra from the fitting to models of ZFS interaction distribution: (a) ZAS, C_5 (solid) and C_3 (dashed); (b) ZDT, C_5 (solid) and C_3 (dashed); (c) ZST, uncorrelated G; and (d) ZCT, C_5. The vertical lines mark the fields at which $g_{\text{eff}} = 9$, 4.3, 2.6, and 2.0.

where the over-bar denotes mean values. This Gaussian distribution is not derived from assumptions about the properties of the sample, therefore it does not directly convey structural information. Nevertheless, since normal distribution of the interaction tensor components is only consistent with C_n distributions and statistical isotropy is only consistent with the Gaussian isotropic model C_5, a Gaussian distribution of D and λ, as opposed to the D_{ij} components, necessarily implies the presence of a certain amount of order.

Results

The X-band spectra of ZAS, ZDT, ZST, and ZCT, recorded at 110 K, are reported in Figure 1, left. They are similar to the spectra already reported in the literature. Several common features can be discerned, which are now briefly enumerated: a broad line centered at $g_{\text{eff}} = 2.0$; a poorly resolved feature occurring at $g_{\text{eff}} \cong 2.6$; a relatively sharp line centered at $g_{\text{eff}} = 4.3$ accompanied by a broad shoulder down to $g_{\text{eff}} \cong 8 \div 9$; a small peak extending from $g_{\text{eff}} \cong 10$ to zero field. In the ZDT and ZST spectra the typical 6-line pattern of impurity Mn^{2+} can be seen. Spectra have also been recorded at higher temperatures, up to 390 K (data not shown). The amplitude of the $g_{\text{eff}} = 4.3$ peak approximately follows Curie's law down to 200 K. At lower temperatures the amplitude is smaller than predicted by Curie's law, as already observed.[11] This behavior is consistent with the well-known fact that the $g_{\text{eff}} = 4.3$ peak arises from the transition within the middle doublet of the m_S manifold of a rhombically distorted Fe(III) ion.[27] The amplitude of the $g_{\text{eff}} = 2.0$ peak decreases with increasing temperature but it does not follow Curie's law, as expected for a peak that is the superposition of many lines associated with different transitions within the m_S manifold.

TABLE 1: Results of the Fit of X-band Spectra to the Models Involving ZFS Parameter Distribution[a]

catalyst	ZFS distribution	fit parameters	D_{peak}/GHz	K^b
ZAS	C_5	$\sigma_5 = (1.27 \pm 0.07)$ GHz	2.4 ± 0.1	0.85
	C_3	$\sigma_3 = (1.93 \pm 0.09)$ GHz	2.5 ± 0.1	
ZDT	C_5	$\sigma_5 = (1.63 \pm 0.09)$ GHz	3.0 ± 0.2	0.15
	C_3	$\sigma_3 = (2.43 \pm 0.10)$ GHz	3.2 ± 0.1	
ZST	uncorrelated G	$\sigma_D = (0.8008 \pm 0.0001)$ GHz, $\bar{D} = (3.04 \pm 0.11)$ GHz $\sigma_\lambda = (0.0009 \pm 0.0001)$, $\bar{\lambda} = (0.77 \pm 0.06)$	[c]	
ZCT	C_5	$\sigma_5 = (1.82 \pm 0.06)$ GHz	3.4 ± 0.1	0.014

[a] Reported uncertainty is the 90% confidence level as estimated by the Monte Carlo bootstrap method with 101 samples. D_{peak} is the point at which the ZFS distribution integrated over all λ values reaches its maximum value. K ($0 \le K \le 1$) is the significance from Kuiper's test. It is the probability that the two observed fit residual distributions are realizations of the same underlying distribution. K is small when two fits have largely different quality and is close to 1 when they have similar quality [b] Refers to the comparison of the fits based on the C_5 and C_3 models. [c] In this case $D_{\text{peak}} = \bar{D}$.

The spectra have been fitted with all the above models (C_5, C_3, and both correlated and uncorrelated G). By comparing the results, the ZFS distribution(s) that best reproduces the experimental spectral shape can be selected. Such selected results are shown in Table 1 and in Figures 1 and 2. The spectral shape is reasonably well reproduced for all catalysts, even if the $g_{\text{eff}} = 4.3$ peak is always less sharp than it should be. This is probably due to the simplified line shape model used (see Appendix). It turned out that the steamed ZST catalyst is best described by an uncorrelated Gaussian distribution of D and λ, whereas the ZAS, ZDT, and ZCT spectra can be well fit to the C_5 model. It is however interesting to note that the C_3 model can also reproduce the ZAS and ZDT spectra (ZCT is only poorly reproduced). This can be visually appreciated from Figure 1. To get a significant quantitative comparison of the performance of the two models, we have to resort to a significance analysis of the distribution of the fit residuals, namely to Kuiper's test[46] (see Table 1). It turns out that, compared to C_5, the C_3 model performs equally well in ZAS, less well in ZDT, and much worse in ZCT.

The various σ values reported in Table 1 are the actual fit parameters. Recall that σ values from different ZFS distributions cannot be directly compared because of the different distribution shape. The σ_5 values, which can be directly compared, show a steady increase ZAS < ZDT < ZCT. The σ_D value for the ZST catalysts is lower and it surely denotes a narrower ZFS distribution despite its different definition since the G distribution has a more "peaked" shape than the C_n distributions (see Figure 2a−d). Although the value of σ_λ in ZST is very low, it is a true minimum of the error function, as checked by repeating the fitting procedure from widely different initial guesses. However, being the λ step in the stick spectra library 0.0125, this value means that only the stick spectra with $\lambda = 0.77$ actually enter the final computed result. The fit parameter errors, estimated at the 90% confidence level, show the good reliability of the fit results. However, the estimated error on σ_D and (in absolute sense) on σ_λ in ZST is very low. Then, we also computed an upper limit for these errors by computing the target function (i.e., the sum of the squared residuals) in an interval about the optimized parameter of interest. Assuming that errors are normally distributed, which is not the actual case since our models are not exact, makes the calculated 90% confidence error an upper limit to the true error. Such limits are 0.004 GHz for

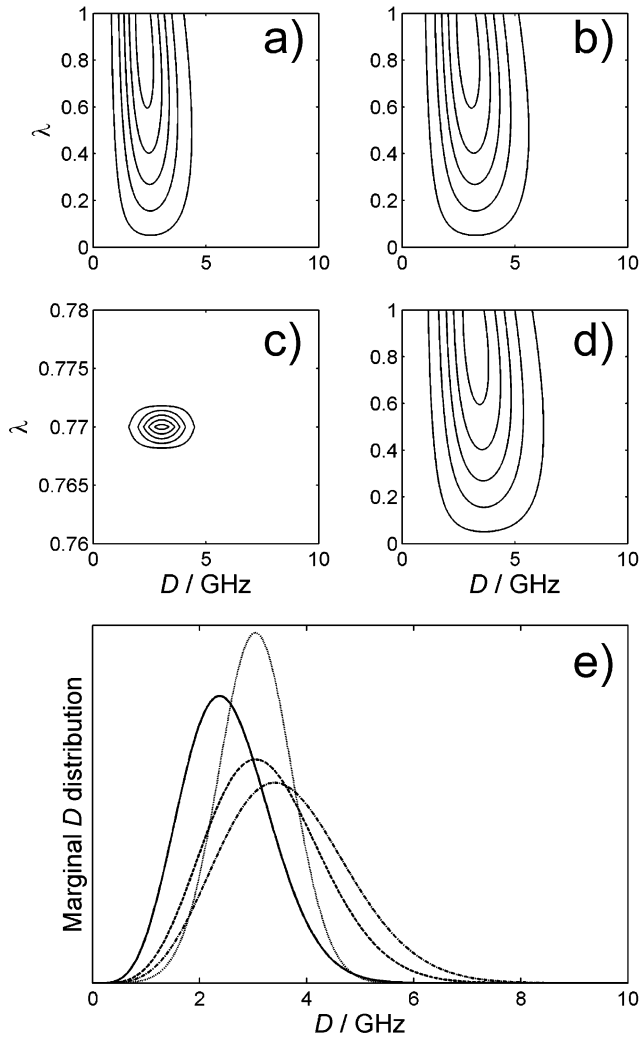

Figure 2. ZFS interaction distribution functions obtained form the fitting of X-band EPR spectra of Fe(III)-doped MFI zeolite at various stages of the treatment sequence. Two-dimensional (D, λ) distributions, normalized to unit area, are shown as contour plots: (a) ZAS, C_5; (b) ZDT, C_5; (c) ZST, uncorrelated G; and (d) ZCT, C_5. Marginal D distributions obtained from the two-dimensional distributions by integrating over λ are shown in panel e: solid line, ZAS; dashed line, ZDT; dotted line, ZST; and dash−dotted line, ZCT. These one-dimensional distributions peak at the D_{peak}.

σ_D and 0.003 for σ_λ. Therefore, σ_λ is barely significant, as expected since, as we have just seen, the computed spectrum will not vary until σ_λ becomes of the order of 0.01. Conversely, σ_D is statistically significant and its error is small because the target function is very sensitive to changes in σ_D.

The derived D_{peak} value is the mode of the marginal D distribution, i.e., the distribution obtained after integration of the two-dimensional ZFS distribution over λ (see Figure 2e). Its physical significance will be discussed in the next section. The point here is that D_{peak} is independent of the underlying ZFS distribution. Therefore, the equality (to within the estimated error) of the D_{peak} values obtained with the C_5 and the C_3 distributions for the ZAS and ZDT catalysts corroborates the consistency of the two different descriptions of the same spectra.

The Q-band spectra of the studied catalysts, recorded at 90 K, are reported in Figure 3, left. They show a single line, centered at $g_{eff} = 2.0$ and 50−60 mT wide. The typical 6-line pattern of Mn^{2+} can again be seen with ZDT, ZST, and ZCT. The Q-band spectra do not show enough structure to completely determine the fitting problem. The best that one can do is to fit

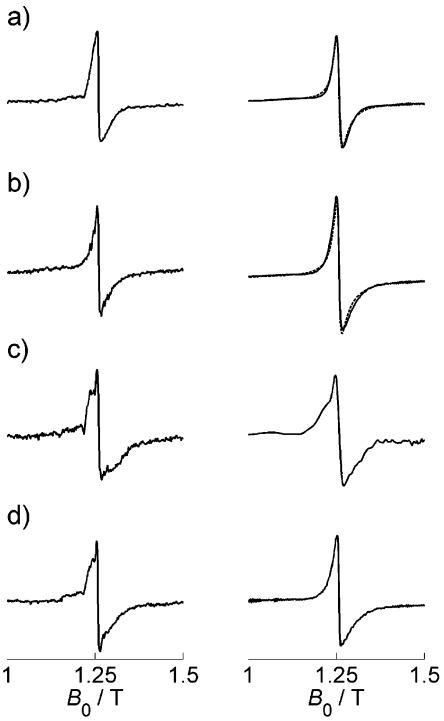

Figure 3. Q-band EPR spectroscopy of Fe(III)-doped MFI zeolite at various stages of the treatment sequence. (Left) Experimental spectra recorded at 90 K (other conditions can be found in the text). (Right) Corresponding spectra computed with the optimized parameters ZFS interaction parameters obtained from the correspondent X-band spectra: (a) ZAS; (b) ZDT; (c) ZST; and (d) ZCT.

the Q-band spectra holding the ZFS distribution parameters fixed, i.e., the optimized parameters are the line width and the (trivial) scaling parameters. The results of such constrained fits are shown in Figure 3, right. It can be seen that the Q-band spectra are consistent with the ZFS distribution parameters obtained from fitting the X-band spectra.

Selected high-frequency spectra recorded at 5 K are reported in Figure 4 for ZAS only, as the other catalysts show very similar response. Up to three lines are observed, but only that at $g = 2.0$ is due to Fe(III) ions. The other ones, resonating at lower fields, belong to the spectrum of triplet-state dioxygen in solid air.[47] The $g = 2.0$ line cannot be observed at 345 and 475 GHz due to magnet limitations and the corresponding spectra are not reported in Figure 4. It consists of a narrow and a broad component, the latter being only observed at frequency ≥190 GHz. The line shape is slightly asymmetric. The line width of the narrow component is 0.01 T, and is almost independent of the microwave frequency, whereas that of the broader component increases almost linearly with frequency from ∼0.3 T at 190 GHz to ∼0.5 T at 285 GHz.

Discussion

The above presented data clearly show that the ZFS interaction of Fe(III) ions in MFI zeolitic catalysts is largely inhomogeneous in nature even just after synthesis and that subsequent high-temperature treatments make this inhomogeneity larger.

The fitting of the X-band CW-EPR spectra of the presently studied catalyst to models of distribution of the ZFS interaction provide detailed insight into inhomogeneity of the environment where the Fe(III) ions reside. Such insight is provided by the analysis of three items resulting from the comparative fitting of the experimental spectra: (i) the performance of the various ZFS distributions; (ii) the peak value D_{peak} of the optimized

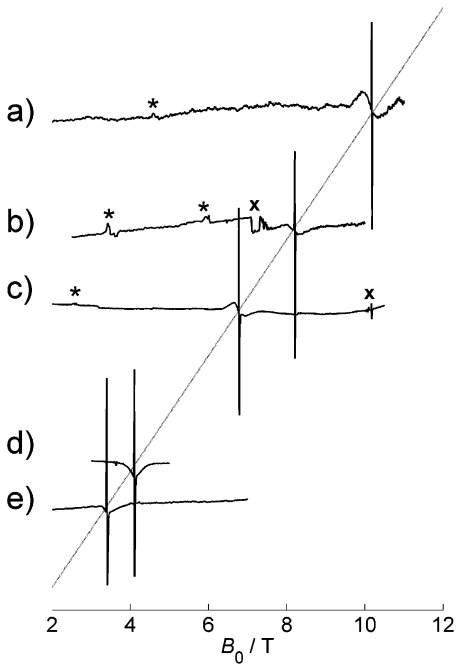

Figure 4. High-frequency EPR spectroscopy of Fe(III)-doped MFI zeolite ZAS (as synthesized) at 5 K (other conditions can be found in the text) at the following excitation frequencies: (a) 285, (b) 230, (c) 190, (d) 115, and (e) 95 GHz. The dashed line marks the $g = 2.0$ line position. Lines due to triplet dioxygen in solid air are denoted by an asterisk and spectrometer artifacts by a cross.

marginal D distribution; and (iii) the width σ of the optimized ZFS distribution.

The spectra of ZAS, ZDT, and ZCT are well reproduced by the C_5 distribution. From a structural point of view this means that (a) the principal axes of the ZFS tensors are isotropically distributed when the whole sample is taken into account, i.e., that our sample is a truly random poly-crystalline powder, and (b) that the components of the ZFS tensors in the sample, expressed in the laboratory frame of reference, are distributed according to a multivariate, uncorrelated Gaussian distribution. Whereas point a is trivial, point b means that there exists inhomogeneity of the ZFS interaction, that this inhomogeneity can be quantified by the σ parameters, and that it is due to the additive contribution of many small deviations from the mean. The existence of ZFS inhomogeneity in crystalline materials and even in the as-synthesized ZAS catalyst may be understood considering that many different lattice sites are accessible to Fe(III) ions. Indeed, there are 12 or 24 different (but similar) tetrahedral sites in the perfect lattice, depending on temperature and the presence of a template,[28,29] and additional inhomogeneity arises from the random distribution of aluminum ions and of lattice defects. Of course, when Fe(III) ions are present in extra-lattice sites and perhaps in clusters of various nuclearity, ZFS inhomogeneity is expected.

The C_3 distribution reproduces the spectra of the ZAS, ZDT, and ZCT catalysts with rapidly decreasing quality ZAS > ZDT > ZCT. One could argue that this just means that these spectra are not sensitive to the presence of local order, as implied by the C_3 distribution. However the smooth performance decrease from ZAS to ZCT, the consistency of the two D_{peak} values for ZAS and ZDT, and the inconsistency for ZCT (the poor C_3 fit of ZCT yields $\sigma_3 = 2.35$ GHz and $D_{peak} = 3.1$ GHz) strongly suggest that the observed behavior is due to a decreasing presence of locally ordered Fe(III) species in the ZAS, ZDT, and ZCT catalysts. Since Fe(III) in lattice sites sees a more ordered environment than it does in extra-lattice ones, and since almost all of the Fe(III) ions in the ZAS catalyst are in lattice sites, we can infer that a certain amount of Fe(III) ions in ZDT is still within the lattice, whereas much more Fe(III) ions are in extra-lattice positions in the ZCT catalysts.

The ZST spectrum is best reproduced by an uncorrelated G distribution. Even if this does not allow us to draw structural conclusions, it is certain that in this catalyst the environment of Fe(III) ions is much more homogeneous than that in the other catalysts. Even if it is unlikely that a single Fe(III) species exists in this catalysts, there probably is a dominating species produced by the steam treatment.

This discussion is further substantiated and detailed by the numerical fit results in Table 1. The D_{peak} values are a measure of the "average strength" of the ZFS interaction, irrespective of nonaxial distortions. The D_{peak} shows a clear step up in going from ZAS to ZDT, as also shown in Figure 2e, but after that it grows much more slowly (ZAS $\ll$ ZDT $\cong$ ZST $<$ ZCT). The strength of the ZFS interaction depends on the strength of the ligand field, that is on the environment of the Fe(III) ions. The average ZFS interaction therefore shows an essential change as soon as a high-temperature treatment is applied to the catalyst, and is afterward almost constant. It is noteworthy that such near-constancy is obtained from very different distributions such as those fitting to the ZDT, ZST, and ZCT spectra. The origin of the increased ZFS strength is not, however, clear since the ZFS interaction depends on either the Fe−O distance or the basicity of the oxygen ligands.

Last, we consider the distribution widths σ. The directly comparable values σ_5 for ZAS, ZDT, and ZCT show an increase from ZAS to ZCT of the ZFS distribution width, i.e, of the inhomogeneity of the Fe(III) sites which accompanies the increase in average ZFS interaction. The width σ_D in the case of ZST cannot be directly compared with the σ_5 values, but it is so small that it surely denotes a narrower ZFS distribution, as also can be appreciated from Figure 2. This means that in ZST there is a substantial decrease in inhomogeneity, i.e., on average the Fe(III) ions feel a more similar environment.

The high-frequency (35−475 GHz) spectra do not show, in addition to the $g_{eff} = 2.0$ line (composite at excitation frequency 190 GHz or higher), any resolved feature typical of ZFS interaction in the temperature range from 5 to 100 K. Similar behavior has been observed at Q-band in Fe(III)-doped $AlPO_4$-5 molecular sieve[48] and at higher frequency in the related Fe(III)-doped MCM-41 mesoporous silica.[49] Although the dependence of the line width on the excitation frequency also suggests that a field-dependent interaction is responsible for this broadening, it can be calculated that such a width can accommodate unresolved ZFS interactions up to about 10 GHz. As a consistency check, the high-frequency spectra could be fitted to the ZFS distributions optimized at X-band. Therefore, the Q-band and high-frequency spectra corroborate the X-band results in that they provide evidence of the absence of ZFS interactions of the order of tens of GHz or larger, at least within the capability of CW-EPR spectroscopy. It can be therefore concluded that the ZFS interaction of Fe(III) ions in MFI zeolite ranges between 1 and 4 to 6 GHz, depending on sample history. The average ZFS strength is between 2.5 and 3.5 GHz, again according to sample history.

On the basis of the above discussion, the fate of Fe(III) in MFI zeolite during the applied treatment sequence can be so envisaged. Just after synthesis (ZAS), the overwhelming majority of the Fe(III) ions reside in lattice sites substituting for silicon. After detemplation/ion-exchange/calcination (ZDT), a

certain fraction of the Fe(III) ions is extracted from the lattice since, on one hand, the ZFS distribution shows an essential change but, on the other hand, evidence of noticeable residual order has been observed. Steaming (ZST) sets a larger fraction of iron ions into extra-lattice sites as (hydr)oxidic aggregates as shown by the dramatic change in ZFS distribution, which, however, has an average strength close to that observed in ZDT. Last, chemical treatment with aqueous $Na_2S_2O_4$/NaCl, followed by ion-exchange and calcination, disperses the Fe(III) into mostly mononuclear (hydr)oxidic ions as shown by the restoration of the ZFS distribution shape to that observed with the ZDT catalyst; the increase of the ZFS parameters can be attributed to more extensive extraction of iron from the lattice brought about by the two last high-temperature treatments.

Conclusions

The present multifrequency (9−475 GHz) CW-EPR study of Fe(III)-doped MFI zeolite has provided clear evidence of the presence of substantial inhomogeneity of the ZFS interaction. The implementation of an algorithm to fit the X-band experimental spectra to ZFS distribution models enabled us to obtain quantitative measures of the ZFS distribution features and their associated errors. Spectra recorded at higher frequency provided a useful consistency check of the results of the analysis of X-band spectra. The changes occurring in the ZFS interaction enabled us to draw structural conclusions regarding Fe(III) ions that can be summarized as follows. Fe(III) ions reside within the lattice in the as-synthesized catalyst. The first high-temperature treatments (detemplation and calcinations) extract a fraction of the Fe(III) ions and set them in extra-lattice sites mostly as isolated ions. High-temperature treatment with steam further extracts Fe(III) from the lattice and leads to an agglomeration of the extra-lattice ions. Finally, treatment with aqueous dithionite redisperses the Fe(III) in the zeolitic channels, again mostly as isolated ions.

Although considerable insight into the nature and behavior of Fe(III) ions in MFI zeolite has been gained by the conventional CW-EPR technique, we plan to report on pulse EPR experiments which could provide additional evidence to the present conclusions and new clues for a more detailed description of these important but difficult systems.

Appendix. Implementation of the Fitting Algorithm

As is widely known, even the mere powder averaging is a computationally expensive task in the simulation of magnetic resonance line shape of disordered systems. For the present case of CW-EPR spectroscopy of high-spin Fe(III) ions, typical CPU times for a PIII processor (see Table 2) indicate a minimal requirement of about 30 s for a single, powder averaged stick spectrum comprising 1000 orientations, which are barely sufficient to obtain a reasonable powder averaging when the ZFS and the electron Zeeman interactions have the same order of magnitude. To repeat such an average for several thousand (D, λ) pairs, one needs several days of CPU time. Clearly, spectral simulation is hardly affordable, let alone spectral fitting, in the usual way: a new strategy is needed. The strategy we implement in the spectral fitting procedure is as follows: (1) Direct calculation of the resonant fields and transition amplitudes by the eigenfield method[50,51] in Liouville space, thus avoiding resonant field search. (2) Transition indexing in Hilbert space, exploiting the knowledge of the transition fields. (3) Computation of the powder stick spectrum at the temperature of interest by sorting the resonant fields, and computing the amplitude from the transition moments and the Boltzmann factors for a single (D,λ) pair. (4) Actual fitting of the experimental spectrum by convolving the powder stick spectra with the appropriate line shape and width model, averaging the convolved spectra by the chosen distribution functions, and computing the target function to be minimized, e.g., the sum of the squared residuals between the experimental spectrum and the computed one.

TABLE 2: CPU Time (s) Measured on a Linux box (PIII 1 GHz processor) for Running Programs Written in Matlab, Translated in C by Matlab Compiler, and Compiled by the Portland C Compiler[a]

	$D = 1$ GHz		$D = 50$ GHz	
	$N_{or} = 1000$	$N_{or} = 10000$	$N_{or} = 1000$	$N_{or} = 10000$
task field[b]	33.29	330.87	29.26	291.81
task stick[c]	1.15	103.22	0.33	16.66
total	1034.44	10434.09	1029.59	10308.47

[a] Parameters: $\nu_{mw} = 9.36$ GHz, B_0 from -5 to 1050 mT in 512 points, $\lambda = 1$, number of orientations N_{or} and D values as indicated. Whereas the task field scales almost linearly with the number of orientations, the task stick scales almost quadratically with the number of transitions in the EPR spectrum, which is 15 N_{or} for $D \ll \nu_{mw}$ and 5 N_{or} for $D \gg \nu_{mw}$. [b] Task field comprises the calculation of resonant fields and transition matrix elements and transition indexing. [c] Task stick comprises the calculation of the stick spectrum by sorting and binning the resonant fields.

Steps 1 and 2 are repeated for each orientation and for each choice of the (D,λ) pair, and the results are permanently stored on disk, thus forming a library of transition fields, amplitudes, and indices for the Hamiltonian in eq 1. Note that the transition amplitude is averaged over all directions perpendicular to the direction of the static field $\mathbf{B}_0$.

Step 3 is repeated for each choice of the (D,λ) pair and temperature, and the results are permanently stored on disk, thus forming a library of powder stick spectra for the spin Hamiltonian in eq 1. For the present calculations a library of 8181 stick spectra computed for 101 D values between 0 and 10 GHz ($\delta D = 0.1$ GHz) and for 81 λ values between 0 and 1 ($\delta\lambda = 0.0125$) has been used. The ZFS distributions for the studied samples negligibly extend beyond $D = 10$ GHz.

Step 4 is performed by the Nelder−Mead simplex algorithm,[52] which has some advantages over gradient methods such as the Levenberg−Marquardt one. The former is much more robust, i.e., it samples the error surface more widely, and does not require the somewhat tricky calculation of numerical derivatives of the target function. Although it is slower than gradient methods, the fitting of EPR spectra of Fe(III) ions in MFI zeolite by the simplex method has always been completed within 30 min, and often much less. The usual argument in favor of gradient methods, that is the estimation of the error on parameters they yield, is in this case weak. Indeed, since our models are with great probability not exact, the fit residuals comprise errors (either systematic and random) which are not normally distributed, thereby invalidating the key assumption underlying parameter error estimation based on the (co)variance matrix. Neglecting this point would produce incorrectly large errors on parameters. In the present case, errors on parameters at the 90% confidence level have been estimated by the Monte Carlo bootstrap method[46] with 101 samples.

To keep the computation time within affordable limits, the number of parameters to be optimized must be kept reasonably low. As we have seen, the probability distribution functions C_5, C_3, and G contain only 1 to 5 parameters. Conversely, line width parameters are very many in principle since line width is related in an unknown way to both ZFS principal values and axes. Since this would make the fit procedure long, difficult, and probably

underdetermined, in Step 4 the stick spectra are first averaged over the chosen distribution and then the total stick spectrum is convoluted with a Lorentzian line shape with width given by the simple model[27]

$$W(B_r) = \tilde{W}_1 \frac{B_r}{\nu_{mw}} + W_2 \qquad (5)$$

where $W(B_r)$ is the width for the line(s) at the resonant field B_r, ν_{mw} is the microwave frequency, $\tilde{W}_1$ is the constant width in the frequency domain, and W_2 is the constant width in the field domain.

This somewhat simplistic line width model is the main limitation of the present spectral fit procedure.

References and Notes

(1) Suzuki, E.; Makashiro, K.; Ono, Y. *Chem. Lett.* **1988**, 953.
(2) Gubelmann, M. H.; Tirel, P. J. France Patent No. 2630735, 1988.
(3) Kharitonov, A. S.; Aleksandrova, T. N.; Vostrikova, L. A.; Sobolev, V. I.; Ione, K. G.; Panov, G. I. USSR Patent No. 1805127, 1988.
(4) Panov, G. I. *Cattech* **2000**, *4*, 18.
(5) Ribera, A.; Arends, I. W. C. E.; de Vries, S.; Perez-Ramirez, J.; Sheldon, R. A. *J. Catal.* **2000**, *195*, 287.
(6) Volodin, A. M.; Dubkov, K. A.; Lund, A. *Chem. Phys. Lett.* **2001**, *333*, 41.
(7) Kotasthane, A. N.; Shiralkar, V. P.; Hegde, S. G.; Kulkarni, S. B. *Zeolites* **1986**, *6*, 253.
(8) Calis, G.; Frenken, P.; Boer, E. d.; Swolfs, A.; Hefni, M. A. *Zeolites* **1987**, *7*, 319.
(9) Kucherov, A. V.; Slinkin, A. A. *Zeolites* **1988**, *8*, 110.
(10) Lin, D. H.; Coudurier, G.; Vedrine, J. C. In *Zeolites: Facts, Figures, Future*; Jacobs, P. A., Santen, R. A. v., Eds.; Elsevier: Amsterdam, The Netherlands, 1989; p 1431.
(11) Bruckner, A.; Luck, R.; Wieker, W.; Fahlke, B.; Mehner, H. *Zeolites* **1992**, *12*, 380.
(12) Goldfarb, D.; Bernardo, M.; Strohmaier, K. G.; Vaughan, D. E. W.; Thomann, H. *J. Am. Chem. Soc.* **1994**, *116*, 6344.
(13) Bordiga, S.; Buzzoni, R.; Geobaldo, F.; Lamberti, C.; Giamello, E.; Zecchina, A.; Leofanti, G.; Petrini, G.; Tozzola, G.; Vlaic, G. *J. Catal.* **1996**, *158*, 486.
(14) Weckhuysen, B. M.; Wang, D. J.; Rosynek, M. P.; Lunsford, J. H. *Angew. Chem. Int. Ed.* **1997**, *36*, 2374.
(15) Brabec, L.; Jeschke, M.; Klik, R.; Novakova, J.; Kubelkova, L.; Meusinger, J. *J. Appl. Catal. A-Gen.* **1998**, *170*, 105.
(16) Kucherov, A. V.; Kucherova, T. N.; Slinkin, A. A. *Microporous Mesoporous Mater.* **1998**, *26*, 1.
(17) Kucherov, A. V.; Montreuil, C. N.; Kucherova, T. N.; Shelef, M. *Catal. Lett.* **1998**, *56*, 173.
(18) Volodin, A. M.; Sobolev, V. I.; Zhidomirov, G. M. *Kinet. Catal.* **1998**, *39*, 775.
(19) El-Malki, E. M.; van Santen, R. A.; Sachtler, W. M. H. *J. Phys. Chem. B* **1999**, *103*, 4611.
(20) Long, R. Q.; Yang, R. T. *J. Catal.* **2000**, *194*, 80.
(21) El-Malki, E. M.; van Santen, R. A.; Sachtler, W. M. H. *J. Catal.* **2000**, *196*, 212.
(22) Fejes, P.; Nagy, J. B.; Lázar, K.; Halász, J. *Appl. Catal. A-Gen.* **2000**, *190*, 117.
(23) Chen, H. Y.; El-Malki, E. M.; Wang, X.; van Santen, R. A.; Sachtler, W. M. H. *J. Mol. Catal. A-Chem.* **2000**, *162*, 159.
(24) Kucherov, A. V.; Nissenbaum, V. D.; Kucherova, T. N.; Kustov, L. M. *Kinet. Catal.* **2002**, *43*, 711.
(25) Kubanek, P.; Wichterlova, B.; Sobalik, Z. *J. Catal.* **2002**, *211*, 109.
(26) Berlier, G.; Spoto, G.; Fisicaro, P.; Bordiga, S.; Zecchina, A.; Giamello, E.; Lamberti, C. *Microchem. J.* **2002**, *71*, 101.
(27) Pilbrow, J. R. *Transition Ion Electron Paramagnetic Resonance*; Clarendon Press: Oxford, UK, 1990.
(28) Koningsveld, H. v.; Bekkum, H. v.; Jansen, J. C. *Acta Crystallogr. B* **1987**, *43*, 127.
(29) Koningsveld, H. v.; Jansen, J. C.; Bekkum, H. v. *Zeolites* **1990**, *10*, 235.
(30) Le Caër, G.; Brand, R. A. *J. Phys.-Condens. Matter* **1998**, *10*, 10715.
(31) Kharitonov, A. S.; Panov, G. I.; Sheveleva, G. A.; Pirutko, L. V.; Voskresenskaya, T. P.; Sobolev, V. I. U.S. Patent No. 5672777, 1997.
(32) Ponti, A. *J. Magn. Reson.* **1999**, *138*, 288.
(33) Hodgkinson, P.; Emsley, L. *Prog. Nucl. Magn. Reson. Spectrosc.* **2000**, *36*, 201.
(34) Eden, M. *Concepts Magn. Reson. Part A* **2003**, *18A*, 24.
(35) Ratnasamy, P.; Kumar, R. *Catal. Today* **1991**, *9*, 329.
(36) Meloni, D.; Monaci, R.; Solinas, V.; Berlier, G.; Bordiga, S.; Rossetti, I.; Oliva, C.; Forni, L. *J. Catal.* **2003**, *214*, 169.
(37) Gromov, I.; Shane, J.; Forrer, J.; Rakhmatoullin, R.; Rozentzwaig, Y.; Schweiger, A. *J. Magn. Reson.* **2001**, *149*, 196.
(38) Weil, J. A.; Bolton, J. R.; Wertz, J. E. *Electron Paramagnetic Resonance*; Wiley: New York, 1994.
(39) Czjzek, G.; Fink, J.; Gotz, F.; Schmidt, H.; Coey, J. M. D.; Rebouillat, J.-P.; Lienard, A. **1981**, *23*, 2513.
(40) Yahiaoui, E. M.; Berger, R.; Servant, Y.; Kliava, J.; Dugunov, L.; Mednis, A. *J. Phys.-Condens. Matter* **1994**, *6*, 9415.
(41) Czjzek, G. *Phys. Rev. B* **1982**, *25*, 4908.
(42) Legein, C.; Buzare, J. Y.; Jacoboni, C. *J. Non-Cryst. Solids* **1995**, *184*, 160.
(43) Legein, C.; Buzare, J. Y.; Emery, J.; Jacoboni, C. *J. Phys.-Condens. Matter* **1995**, *7*, 3853.
(44) Legein, C.; Buzare, J. Y.; Boulard, B.; Jacoboni, C. *J. Phys.-Condens. Matter* **1995**, *7*, 4829.
(45) Kliava, J.; Berger, R.; Servant, Y.; Emery, J.; Greneche, J. M.; Trokss, J. *J. Non-Cryst. Solids* **1996**, *202*, 205.
(46) Press, W. H.; Teukolsky, S. A.; Vetterling, W. T.; Flannery, B. P. *Numerical Recipes*, 2nd ed.; Cambridge University Press: Cambridge, 1995.
(47) Pardi, L. A.; Krzystek, J.; Telser, J.; Brunel, L. C. *J. Magn. Reson.* **2000**, *146*, 375.
(48) Brückner, A.; Lohse, U.; Mehner, H. *Microporous Mesoporous Mater.* **1998**, *20*, 207.
(49) Konovalova, T. A.; Gao, Y. L.; Kispert, L. D.; van Tol, J.; Brunel, L. C. *J. Phys. Chem. B* **2003**, *107*, 1006.
(50) Belford, G. G.; Belford, R. L.; Burkhalter, J. F. *J. Magn. Reson.* **1973**, *11*, 251.
(51) Cugunov, L.; Mednis, A.; Kliava, J. *J. Magn. Reson. Ser. A* **1994**, *106*, 153.
(52) Nelder, J. A.; Mead, R. *Comput. J.* **1965**, *7*, 308.